Enhanced quantum-confined Pockels effect in SiGe superlattices

Pu Yu, Jian Wu, and Bang-Fen Zhu

Department of Physics and Center for Advanced Study, Tsinghua University, Beijing 100084, People's Republic of China
(Received 11 December 2005; revised manuscript received 21 February 2006; published 15 June 2006)

An improved virtual crystal approximation in the empirical pseudopotential formalism is proposed with the accumulated strain effect taken into proper account. Then as applied to the long-period trilayer superlattices, $Si/Si_{0.75}Ge_{0.25}/Si_{0.5}Ge_{0.5}$, the enhanced optical anisotropy in this strained structure in the presence of an external electric field, namely, the giant quantum confined Pockels effect, is confirmed. This enhanced Pockels effect is attributed to the type-II indirect optical transitions associated with two different chemical bonds with different orientations at the $Si_{0.5}Ge_{0.5}$-Si interface. Varying the structure parameters, the dependence of the Pockels coefficient on the thickness of each constituent layer is explained, and the optimized structure is obtained. Moreover, a new structure, the graded-Si_xGe_{1-x}/Si superlattice with varying profiles of x in the graded layers, is proposed, in which the whole graded region can contribute to the Pockels effect; thus a Pockels coefficient as large as 10^{-9} cm/V is predicted. Three types of graded-Si_xGe_{1-x}/Si superlattices, i.e., the x profile as functions of sawtooth, parabola, and antiparabola, are investigated, and the most promising structure is obtained, and explained by the competition between the quantum confinement of carriers and the spatial variation rate of the composition x in graded layers.

I. INTRODUCTION

Recently, optical nonlinearity in low-dimensional systems has become a rapidly growing field in both the fundamental physics and technical applications. With the development of crystal growth techniques, there have been continuous efforts towards realizing the next generation of optoelectronic devices by engineering the electronic and optical properties,[1–5] in particular the second order optical nonlinearity, which is crucial for modulation, switching in optoelectronics circuits, and phase matching in nonlinear optics.[6] So far, however, most of researches on this topic have focused on the III-V semiconductor system,[7–19] and little has been done on the Si-based heterostructure, because the electro-optic coefficient in bulk Si vanishes due to its O_h point-group symmetry, though a number of research groups have investigated peculiar linear optical properties in some Si-based heterostructures.[20–23]

By breaking the intrinsic inversion symmetry, the heterostructure can be asymmetric and of novel physical properties unavailable in bulk materials. A few years ago, a novel Si-based trilayer heterostructure, $Si/Si_{0.75}Ge_{0.25}/Si_{0.5}Ge_{0.5}$, was proposed by one of the present authors (Zhu) and his co-workers,[24] in which an enhanced Pockels effect, i.e., the electric-field induced biaxial birefringence within the plane perpendicular to the field, was predicted by using the empirical tight-binding (ETB) method. In calculating the momentum matrix elements (MMEs), a technique of taking the k-space gradient of the ETB Hamiltonian is invoked, so that no additional empirical parameters are required.[25,26] However, as recently pointed out in Ref. 27, in this method the intra-atomic term, i.e., the MMEs between different atomic states localized on the same atom, are completely neglected, which in fact does have very important contributions. Thus, a more accurate calculation is required to evaluate the second order optical nonlinearity in such a kind of heterostructure. Among various methods for energy band calculation, we

choose the empirical pseudopotential method (EPM), because the MMEs in this method are directly calculated in terms of the plane waves superposing the eigenstates.

In this article, we will apply the EPM to calculating the electronic structure and optical nonlinearity of the Si-based trilayer superlattices, $Si/Si_{0.75}Ge_{0.25}/Si_{0.5}Ge_{0.5}$, suggested in Ref. 24. In order to simplify the calculation, we adapt the virtual crystal approximation (VCA) to this long-period strained structure as the zeroth-order approximate potential. With the enhanced Pockels effect confirmed, the enhancement mechanism is explored and attributed to the type II indirect optical transitions associated with the two different chemical bonds with different orientations at interfaces. Based on this, we propose another set of Si-based heterostructures, the graded-Si_xGe_{1-x}/Si superlattices grown on the (001) Si substrate, in which the Pockels-active region is extended from the interfaces to whole graded layers, so that an even larger Pockels coefficient can be expected. We also suggest the optimized structure for the trilayer and graded superlattices for their optoelectronic applications.

II. METHOD

The EPM is a sophisticated method for the band structure calculation. If the crystal potential of the superlattice can be written as the superposition of the atomic potential V_α with $\mathbf{t}_\alpha$ denoted the coordinate of the atom α in a supercell,[28,29] the single particle Schrödinger equation reads

$$\left[-\frac{\hbar^2}{2m}\nabla^2 + \sum_{\mathbf{R},\alpha} V_\alpha(\mathbf{r} - \mathbf{R} - \mathbf{t}_\alpha) \right] \psi_n(\mathbf{r}) = E_n \psi_n(\mathbf{r}), \quad (1)$$

where $\mathbf{R}$ represents the superlattice vector. Expanding in terms of the plane waves with the reciprocal lattice vectors ($\mathbf{g}$'s) of the superlattice, the matrix elements of Hamiltonian can be expressed as

TABLE I. Parameters of the pseudopotentials for Si and Ge (atomic units, i.e., a_1 in hartree a.u.[3]).

	a_1	a_2	a_3	a_4	a_5	a_6
Si	106.0686	2.2278	0.6060	−1.9720	5.0	0.3
Ge	54.4512	2.3592	0.7400	−0.3800	5.0	0.3

$$H_{\mathbf{g},\mathbf{g}'}(\mathbf{k}) = \frac{\hbar^2(\mathbf{g}+\mathbf{k})^2}{2m}\delta_{\mathbf{g},\mathbf{g}'} + \sum_\alpha e^{-i(\mathbf{g}'-\mathbf{g})\cdot\mathbf{t}_\alpha}V_f^\alpha(|\mathbf{g}'-\mathbf{g}|),$$

(2)

where $V_f^\alpha(|\mathbf{g}'-\mathbf{g}|)$ is the form factor of the atom α associated with the reciprocal lattice vector $\mathbf{g}'-\mathbf{g}$, and $\mathbf{k}$ represents the wave vector of the electron in superlattices.

The form factors of Si and Ge in bulk materials are taken from the expression[30]

$$V_f(|\mathbf{g}|) = \frac{a_1(|\mathbf{g}|^2-a_2)}{e^{a_3(|\mathbf{g}|^2-a_4)}+1}\left[\frac{1}{2}\tanh\left(\frac{a_5-|\mathbf{g}|^2}{a_6}\right)+\frac{1}{2}\right],$$

(3)

where parameters a_i ($i=1,2,3,4,5,6$) are listed in Table I, and $V_f(|\mathbf{g}|)$ are normalized by the cell volume of the crystal.[30] The alloy form factors are chosen as the weighted average of those of the bulks. We note that the band offset has already been included in the form factors $V_f^\alpha(|\mathbf{g}'-\mathbf{g}|=0)$ ($\alpha=$ Si, Ge), thus no additional parameter is needed.

This method has been successfully applied to the short-period superlattices.[31–33] However, its application to the long-period superlattice is restricted by the requirement of huge computer memory and ultralong CPU time which increase with the size of the supercell in the third power. To circumvent this difficulty, the VCA is usually adopted, where the superlattice is treated as the perturbation to an overall virtual crystal,[34] so that a smaller number of plane waves can give rise to the eigenstates near the band gap with reasonable accuracy.

In general, the perturbation potential in the VCA, which represents the difference between the overall virtual crystal and the actual superlattice, can be expressed as

$$\Delta H(\mathbf{r}) = \sum_{\mathbf{g},\alpha} e^{-i\mathbf{g}\cdot(\mathbf{t}_\alpha+\mathbf{r})}V_f^\alpha(|\mathbf{g}|) - \sum_{\mathbf{G},\beta} e^{-i\mathbf{G}\cdot(\tau_\beta+\mathbf{r})}V_0(|\mathbf{G}|), \quad (4)$$

where τ_β labels the coordinate of atom β in the unit cell of the overall virtual alloy of Si and Ge, $\mathbf{G}$ is the reciprocal lattice vector of the virtual crystal. Since the virtual crystal has the same symmetry as the bulk and we are interested only in the bands around the band gap, it is sufficient to expand the eigenfunctions of the zeroth order Hamiltonian by 65 plane waves with different $\mathbf{G}$ vectors. Following the usual procedure, we expand the superlattice eigenstate by wave functions of 20 bands of the virtual alloy (4 valence plus 16 conduction bands) with wave vectors differed by g's. The form factors for the superlattice and virtual alloy are represented as $V_f^\alpha(|\mathbf{g}|)$ and $V_0(|\mathbf{G}|)$, respectively.[30]

This technique works well in calculating the band structure of several types of superlattices, but not for the long-period strained superlattice. In strained superlattices, it is

TABLE II. The band gap of superlattices of $\text{Si}_n/(\text{Si}_{0.75}\text{Ge}_{0.25})_n/(\text{Si}_{0.5}\text{Ge}_{0.5})_n$ calculated with different methods (Unit: eV).

n	12	16	20	24	28	32
A	0.969	0.895	0.824	0.776	0.740	0.711
B	0.976	0.905	0.835	0.778	0.717	0.642
C	0.969	0.895	0.825	0.777	0.742	0.714
Mended VCA	0.970	0.899	0.830	0.786	0.754	0.731
Supercell model	0.969	0.897	0.826	0.778	0.748	0.726

usually assumed that each layer will be expanded or compressed along the growth direction (z axis), while keeping the in-plane lattice constant ($a_\parallel$) equal to that of the substrate. Then, the lattice constant along z axis simply reads[28,29]

$$a_\perp = a_i\left[1-D_i\left(\frac{a_\parallel}{a_i}-1\right)\right],$$

(5)

where a_i is the lattice constant of bulk material, and D_i is the elastic modulus of the corresponding bulk material grown on the substrate (001), which is 0.776 for Si, 0.751 for Ge, and the weighted average for the alloy, respectively. Thus, due to the 4% lattice mismatch between bulk Si and Ge, the atomic positions in the strained superlattice will deviate from that in the virtual crystal, and this deviation will be accumulated and become significant when the period is sufficiently long.

To estimate the error caused by the strain accumulation by using the conventional VCA method, we have calculated the energy band gaps in a set of strained superlattices, $\text{Si}_n/(\text{Si}_{0.75}\text{Ge}_{0.25})_n/(\text{Si}_{0.5}\text{Ge}_{0.5})_n$ with different layer width n, in which the coordinate origin of the supercell is chosen in the middle plane of the Si, $\text{Si}_{0.75}\text{Ge}_{0.25}$, and $\text{Si}_{0.5}\text{Ge}_{0.5}$ layers, respectively, denoted as the A, B, and C configurations in Table II. As shown in the first three lines of the table, when increasing the supercell size, the calculated band gaps with different origin vary substantially, with the largest deviation as large as 10%. However, if the conventional VCA was feasible, the different supercell origins should not affect the band structure. This problem is caused in fact by the highly restricted basis space used in the VCA calculation, in which 20 bands instead of 65 bands are used to reduce computation time.

To overcome the difficulties in VCA caused by the accumulated deviation in the long-period strained superlattices, we propose a mended VCA, in which the zeroth-order Hamiltonian is chosen as

$$H_{\mathbf{G},\mathbf{G}'}^0(\mathbf{g_z}+\mathbf{k}) = \frac{\hbar^2(\mathbf{G}+\mathbf{g_z}+\mathbf{k})^2}{2m}\delta_{\mathbf{G},\mathbf{G}'}$$

$$+ \sum_\alpha e^{-i(\mathbf{G}'-\mathbf{G})\cdot\mathbf{t}_\alpha}V_f^\alpha(|\mathbf{G}'-\mathbf{G}|), \quad (6)$$

where $\mathbf{g_z}$ is the reciprocal lattice vector of the superlattice along the $\mathbf{z}$ direction. In the later calculation, totally 50 $\mathbf{g_z}$'s will be used for the superlattices with a supercell of 100 monolayers.[35] Then, the perturbation potential is

$$\Delta H(\mathbf{r}) = \sum_{\mathbf{g},\alpha} e^{-i\mathbf{g}\cdot(\mathbf{t}_\alpha+\mathbf{r})} V_f^\alpha(|\mathbf{g}|) - \sum_{\mathbf{G},\alpha} e^{-i\mathbf{G}\cdot(\mathbf{t}_\alpha+\mathbf{r})} V_f^\alpha(|\mathbf{G}|). \quad (7)$$

With this prescription, the virtual alloy in the zeroth-approximation is some kind of average over not only the compositions but also the strained atomic positions, whereby the Hamiltonian is independent of the coordinate origin of the supercell.

By taking the wave functions of the virtual crystal as the basis set, i.e., $\phi_n(\mathbf{g}_\mathbf{z}+\mathbf{k})$ with the band index n and wave vector $\mathbf{g}_\mathbf{z}+\mathbf{k}$, the wave function of the superlattice $\psi_i(\mathbf{k})$ can be expanded as

$$\psi_i(\mathbf{k}) = \sum_{n,\mathbf{g}_\mathbf{z}} A_{i,n,\mathbf{g}_\mathbf{z}}(\mathbf{k}) \phi_n(\mathbf{g}_\mathbf{z}+\mathbf{k})$$

$$= \sum_{n,\mathbf{g}_\mathbf{z}} A_{i,n,\mathbf{g}_\mathbf{z}}(\mathbf{k}) \sum_{\mathbf{G}} a_{n,\mathbf{G}}(\mathbf{g}_\mathbf{z}+\mathbf{k}) e^{i(\mathbf{g}_\mathbf{z}+\mathbf{k}+\mathbf{G})\cdot\mathbf{r}}, \quad (8)$$

where the band index for the superlattice is denoted as i. The Hamiltonian matrix elements under the mended VCA can then be expressed as

$$H_{n,\mathbf{g}_\mathbf{z},n',\mathbf{g}_z'}(\mathbf{k}) = E_n(\mathbf{g}_\mathbf{z}+\mathbf{k})\delta_{n,n'}\delta_{\mathbf{g}_\mathbf{z},\mathbf{g}_\mathbf{z}'} + \sum_{\mathbf{G},\mathbf{G}'} a_{n,\mathbf{G}}^*(\mathbf{g}_\mathbf{z}+\mathbf{k})$$

$$\times a_{n',\mathbf{G}'}(\mathbf{g}_\mathbf{z}'+\mathbf{k}) \sum_\alpha e^{-i\Delta\mathbf{g}\cdot\mathbf{t}_\alpha}$$

$$\times V_f^\alpha(|\Delta\mathbf{g}|)(1-\delta_{n,n'}\delta_{\mathbf{g}_\mathbf{z},\mathbf{g}_\mathbf{z}'}), \quad (9)$$

with $\Delta\mathbf{g}=\mathbf{G}'-\mathbf{G}+\mathbf{g}_\mathbf{z}'-\mathbf{g}_\mathbf{z} \equiv \Delta g_1\hat{x}+\Delta g_2\hat{y}+\Delta g_3\hat{z}$.

To examine the validity and efficiency of the mended VCA, the band gaps of the sample superlattices are calculated and compared with the results by the supercell model. As listed in the last two rows of Table II, the band gaps calculated by the mended VCA are very close to those by the supercell model. Furthermore, it should be noted that the time needed for calculating the dispersion relations of structure with $n=32$ by the supercell model is about 40 times of that by the mended VCA. Hence, the mended VCA is proved to be suitable for calculating the long-period strained superlattices with reasonable accuracy.

Now, as an application, we calculate the quantum confined Pockels effect in the Si-based trilayer superlattices, $\mathrm{Si}/\mathrm{Si}_{0.75}\mathrm{Ge}_{0.25}/\mathrm{Si}_{0.5}\mathrm{Ge}_{0.5}$.[24] Unlike bulk Si, the present system has a point-group symmetry of C_{2v}, in which the principal axes of the ellipsoid of the dielectric constant tensor are along the [001], [110], and [$\bar{1}$10] directions, respectively.

When an external electric field F is applied along the superlattice growth direction along the z axis, an additional term eFz is added to the Hamiltonian. For the sake of simplicity, in calculating the energy band structure, the usual truncation approximation for the electric field along the growth direction is adopted,[36,37] i.e., the coupling between the nearest supercells induced by the field is neglected. To minimize the influence of the Gibbs' phenomenon induced by the truncation approximation, we choose the midplane of the barrier ($\mathrm{Si}_{0.75}\mathrm{Ge}_{0.25}$ in trilayer superlattices and Si in graded superlattices) as the electric field truncation position. Then the perturbation due to the electric field in the mended VCA can be written as

$$\Delta H_{n,\mathbf{g}_\mathbf{z},n',\mathbf{g}_\mathbf{z}'}(\mathbf{k}) = -\sum_{\mathbf{G},\mathbf{G}'} a_{n,\mathbf{G}}^*(\mathbf{g}_\mathbf{z}+\mathbf{k})a_{n',\mathbf{G}'}(\mathbf{g}_\mathbf{z}'+\mathbf{k})$$

$$\times\left[\left(\frac{iL_z}{2\Delta g_3}+\frac{1}{\Delta g_3^2}\right)e^{-i\Delta g_3 L_z}\right.$$

$$\left.+\left(\frac{iL_z}{2\Delta g_3}-\frac{1}{\Delta g_3^2}\right)\right]\frac{eF}{L_z}\delta_{0,\Delta g_1}\delta_{0,\Delta g_2},$$

$$(10)$$

in which $\Delta g_3 \neq 0$ and L_z is the superlattice period along the $\mathbf{z}$ direction.

With the calculated eigenfunctions of the superlattice, the imaginary part of the dielectric function can be readily obtained through

$$\varepsilon_{\hat{\tau}}(\omega) = \frac{4\pi^2 e^2}{m^2\omega^2}\sum_{\mathbf{k},c,v}|\hat{\tau}\cdot\mathbf{P}_{c,v}(\mathbf{k})|^2\delta(E_v(\mathbf{k})+\hbar\omega-E_c(\mathbf{k})), \quad (11)$$

where $\hat{\tau}$ denotes the unit polarization direction of the incident light with energy $\hbar\omega$, and the momentum matrix element $\mathbf{P}_{c,v}(\mathbf{k})$ can be written as

$$\mathbf{P}_{c,v}(\mathbf{k}) = \frac{m_0}{\hbar}\sum_{n,n',g_z} A_{c,n,g_z}^*(\mathbf{k})A_{v,n',g_z}(\mathbf{k})$$

$$\times\sum_{\mathbf{G}} a_{n,\mathbf{G}}^*(\mathbf{g}_\mathbf{z}+\mathbf{k})a_{n',\mathbf{G}}(\mathbf{g}_\mathbf{z}+\mathbf{k})\mathbf{G}. \quad (12)$$

In later calculation, 145 $\mathbf{k}$ points in one quarter of the mini-zone are used, and the delta function will be replaced by a Lorentzian with a half-width of 20 meV. Through Kramers-Kronig relation the real part of the dielectric function can be obtained,[39] whereby the refractive index along three principal directions, n_{110} (labeled as n_1), $n_{\bar{1}10}$ (n_2), and n_{001} (n_3) are deduced as

$$n_1(F) = n_1(0) - \frac{1}{2}n_1^3(0)(r_{13}+r_{63})F,$$

$$n_2(F) = n_2(0) - \frac{1}{2}n_2^3(0)(r_{13}-r_{63})F,$$

$$n_3(F) = n_3(0) - \frac{1}{2}n_3^3(0)r_{33}F, \quad (13)$$

where r_{13}, r_{63}, and r_{33} are the Pockels coefficients of the system.

III. $\mathrm{Si}/\mathrm{Si}_{0.75}\mathrm{Ge}_{0.25}/\mathrm{Si}_{0.5}\mathrm{Ge}_{0.5}$ TRILAYER SUPERLATTICES

Figure 1 shows the calculated Pockels coefficients in the superlattice $(\mathrm{Si})_{34}/(\mathrm{Si}_{0.75}\mathrm{Ge}_{0.25})_{32}/(\mathrm{Si}_{0.5}\mathrm{Ge}_{0.5})_{34}$. It is seen that, r_{63}, which scales the asymmetric part of the in-plane anisotropic response to the electric field, is equal to 5.8 $\times 10^{-10}$ cm/V, which is significant for optoelectronic applications, confirming the previous conclusion based on ETB calculation qualitatively.[24]

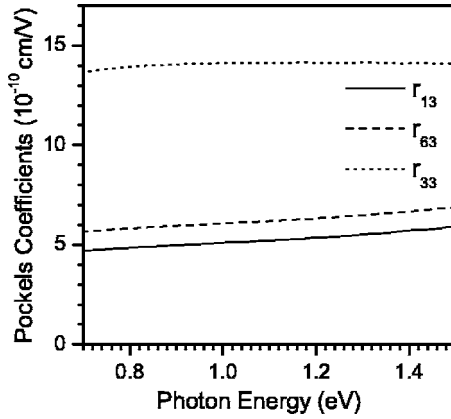Being of the inversion symmetry, all the bulk Si, $\mathrm{Si}_{0.75}\mathrm{Ge}_{0.25}$, and $\mathrm{Si}_{0.5}\mathrm{Ge}_{0.5}$ are not expected to have finite

FIG. 1. The calculated Pockels coefficient for superlattice $(Si)_{34}/(Si_{0.75}Ge_{0.25})_{32}/(Si_{0.5}Ge_{0.5})_{34}$ in an external field of 20 kV/cm along the growth direction.

Pockels effect. It is the broken inversion symmetry in the trilayer structure that is generally responsible for the Pockels effect. The enhanced Pockels coefficient at photon energy less than or about the band gap calculated in this peculiar structure can be understood from its band structure, in particular the type-II band alignment, where electrons and holes are separated spatially, and the different response of the confined electrons and holes to the electric field. As shown in Fig. 2(a), the solid and dashed lines represent the envelope functions of the first hole and electron subbands without electric field, respectively. Obviously, the electrons (holes) are mainly confined to the Si ($Si_{0.5}Ge_{0.5}$) layers, while the $Si_{0.75}Ge_{0.25}$ layers act as the barriers for both electrons and holes. Because only a small portion of the wave function penetrates into the barriers, the present structure has the type-II band alignment, and indirect optical transitions arise only within a narrow region adjacent to the $Si_{0.5}Ge_{0.5}$-Si interfaces. In other words, three types of interfaces between different constituents in this structure are nonequivalent, and the most relevant to the in-plane optical anisotropy is the different chemical bonds associated with different orientations, [110] and [$\bar{1}$10], in two sides of the $Si_{0.5}Ge_{0.5}$-Si interface.

In the presence of an external electric field, electrons and holes will polarize towards opposite directions. As shown in Fig. 2, the envelope functions of the conduction subbands shift to the left, while those of the holes move to the right. The redistribution of the envelope functions changes the electron-hole overlap around the $Si_{0.5}Ge_{0.5}$-Si interface, resulting in the variation of the in-plane anisotropy.

Since the layer thickness plays a dominant role in determining the energy of quantized levels and the wave function penetration, the overlap integral of the electron and hole wave functions around the interfaces in such a type-II quantum structure will also depend on structure parameters, in particular the layer thickness. Thus a systematic study of Pockels coefficients as a function of the layer thickness in the trilayer superlattice is required to find an optimized structure with stronger Pockels effect. Because the size of supercell in strained superlattices must be less than the critical length, we fix the total number of monolayers in a supercell
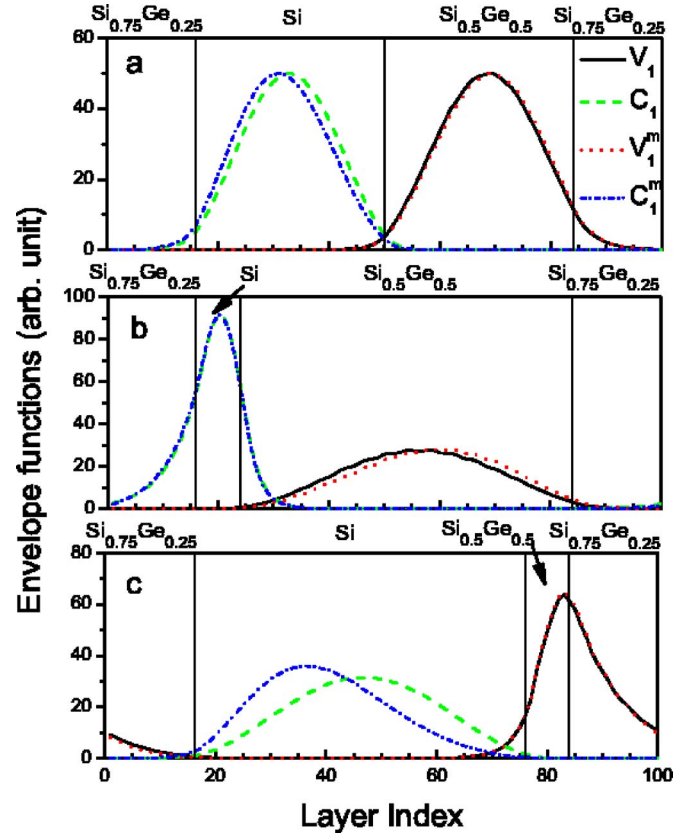

FIG. 2. (Color online) Envelope functions of subbands in three different structures, (a) $(Si)_{34}/(Si_{0.75}Ge_{0.25})_{32}/(Si_{0.5}Ge_{0.5})_{34}$, (b) $(Si)_8/(Si_{0.75}Ge_{0.25})_{32}/(Si_{0.5}Ge_{0.5})_{60}$, and (c) $(Si)_{60}/(Si_{0.75}Ge_{0.25})_{32}/(Si_{0.5}Ge_{0.5})_8$. Here V_1 and C_1 denote the first valence and conduction subband without electric field, respectively; those with the superscript m stand for the subbands in the presence of a longitudinal field of 50 kV/cm.

to be 100. As mentioned above, since the $Si_{0.75}Ge_{0.25}$ layer plays the role of potential barrier for both electrons and holes, its width should be thick enough to confine both the electrons and holes. Hence, we keep the number of monolayers in the $Si_{0.75}Ge_{0.25}$ layer a constant of 32, and the structure to be optimized is $(Si)_n/(Si_{0.75}Ge_{0.25})_{32}/(Si_{0.5}Ge_{0.5})_{68-n}$. The Pockels coefficient r_{63} as a function of the thickness of the Si layer (n) is depicted in Fig. 3 at the photon energy of 0.8 eV (1.55 μm), which corresponds to the canonical wavelength of the transmitting signals through optic fiber cables.[38] It can be seen that r_{63} reaches the maximum value when $n \approx 40$.

The physics behind such a thickness dependence of r_{63} is as follows. First, the penetration of wave function into potential barriers depends on the barrier height, carrier effective mass, and well width. The thinner layer, lower barrier height and lighter mass favor more penetration. Second, the electric field induced polarization of confined carriers depends on the well width and field strength. The thicker well and stronger field result in more significant carrier shift. Three panels in Fig. 2 indicate that, for thin wells, the penetration of the hole into the Si layers is less than the electron's penetration into the $Si_{0.5}Ge_{0.5}$ layers; on the other hand, when the well is thick enough, the penetration of the wave function of the
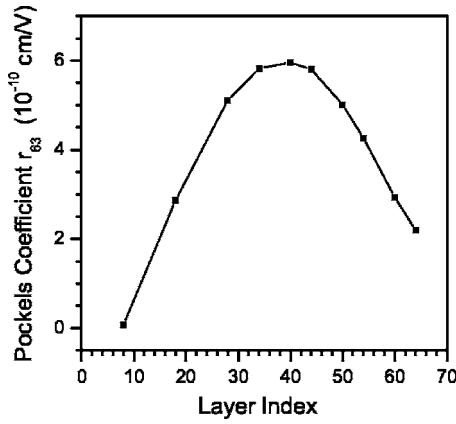
FIG. 3. Calculated Pockels coefficient r_{63} as a function of the number of monolayers in the Si layer at fixed photon energy ($\hbar\omega$ =0.8 eV).

lowest subbands is negligible. As mentioned above, only different types of chemical bonds with different orientation extremely adjacent to the $Si_{0.5}Ge_{0.5}$-Si interface will contribute to the Pockels coefficient. Thus the structure associated with a thicker $Si_{0.5}Ge_{0.5}$ or Si layers as shown in Figs. 2(b) and 2(c) has smaller r_{63}, in spite of that the penetration of another type of carrier is significant, as the interband transition involves both types of carriers. Besides, the maximum value of r_{63} is reached at $n\sim40$, when the Si layer is slightly thicker than that of $Si_{0.5}Ge_{0.5}$, because the confinement of holes to the $Si_{0.5}Ge_{0.5}$ layer is stronger than that of electrons to the Si layer (see Fig. 3).

IV. GRADED-Si_xGe_{1-x}/Si SUPERLATTICES

Stimulated by the fact that the enhanced Pockels effect is mainly contributed by the different chemical bonds with different orientations at the interfaces, we propose a new novel structure for the Pockels effect, i.e., the graded-Si_xGe_{1-x}/Si superlattices. In this system, each monolayer in the graded region Si_xGe_{1-x} links different bonds with varying alloy compositions, thus the Pockels-active region is effectively expanded.

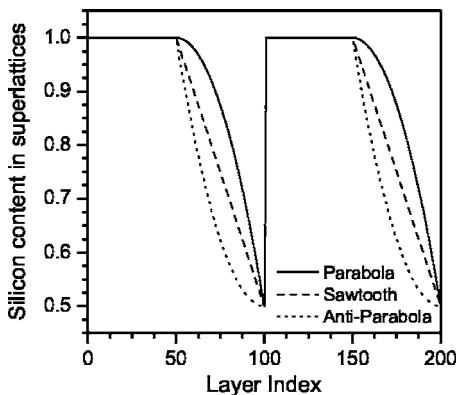As plotted in Fig. 4, three types of graded-Si_xGe_{1-x}/Si

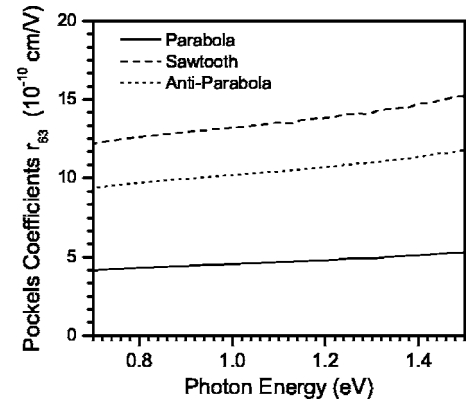FIG. 4. The silicon content profiles in three graded-$(Si_xGe_{1-x})_{50}$/Si_{50} superlattices.

FIG. 5. Calculated Pockels coefficient r_{63} for graded-$(Si_xGe_{1-x})_{50}$/$(Si)_{50}$ superlattices in an external field of 20 kV/cm.

superlattices with different profiles of x are considered, in which among 100 monolayers of each supercell, the first 50 monolayers are pure Si layers while the Si content in the next 50 monolayers varies continuously with the layer index as a function of the sawtooth, parabola, and antiparabola, respectively. Clearly, the inversion symmetry in these structures is broken, and a lower point-group symmetry C_{2v} exists. Since r_{63} has great application potential in the optoelectronics, we focus on it in the following discussion.

Figure 5 shows the Pockels coefficient r_{63} in three different graded-$(Si_xGe_{1-x})_{50}$/$(Si)_{50}$ superlattices as functions of the photon energy. Obviously, the Pockels effect is enhanced in all three cases. At the photon energy of 0.8 eV the calculated Pockels coefficient r_{63} is as large as 9.70×10^{-10} cm/V, 12.61×10^{-10} cm/V, and 4.30×10^{-10} cm/V for the graded layer with the Si content as a function of the antiparabola, sawtooth, and parabola, respectively. This indicates that the sawtooth superlattice performs best in its quantum confined Pockels effect.

Since the band gap for the antiparabola, sawtooth, and parabola-graded superlattices is 0.877 eV, 0.914 eV, and 0.951 eV, respectively, the contribution to the Pockels coefficient around 0.8 eV comes mainly from the optical transitions between several lowest hole and electron subbands. On the other hand, because the electrons are confined to the pure Si layers while holes to the graded-Si_xGe_{1-x}/Si layers, the type II band alignment leads to the spatially indirect optical transitions in the region of interest. Thus, two factors, the overlap integral between wave functions and difference between chemical bonds with different orientations, should be combined to determine the quantum confined Pockels effect quantitatively.

The penetration of wave functions into potential barriers, particularly the penetration of conduction subbands into the Si_xGe_{1-x} layers will affect the indirect transition strength at the graded region. Take the sawtooth graded superlattice as an example. As shown in Fig. 6, the first and second electron subbands are mainly confined to the Si layers which hardly penetrate through the abrupt interface of Si-$Si_{0.5}Ge_{0.5}$. As a result, the overlap integral at the abrupt interface between the confined holes and electrons is negligible. Although the lowest two hole subbands can penetrate through the Si-$Si_{0.5}Ge_{0.5}$ interface significantly, the optical transition in the
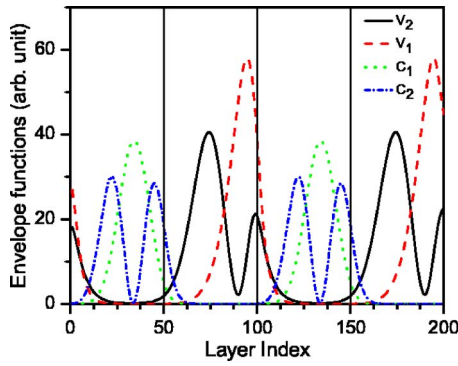
FIG. 6. (Color online) Absolute values of the subband envelope functions in the sawtooth superlattice. The V and C denote the valence and conduction subband and the subscript 1 and 2 stand for the first and second subbands.
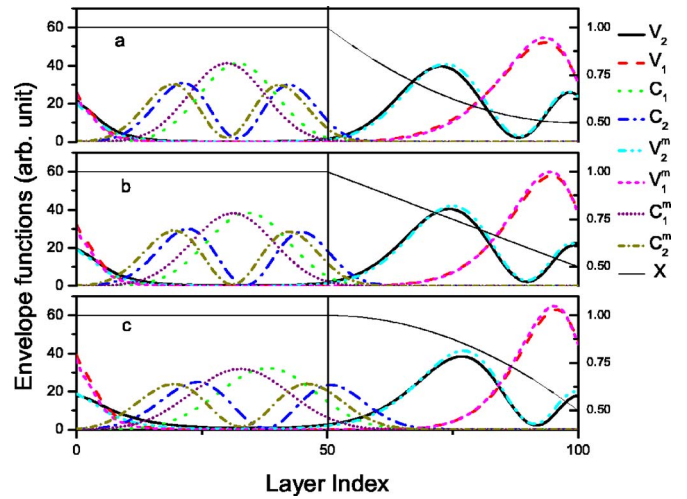

FIG. 7. (Color online) Absolute values for the subband envelope functions in the superlattice with the graded layer profile as the antiparabola (a), sawtooth (b), and parabola (c), respectively. The V and C denote the valence and conduction subband, and the subscript 1 and 2 stand for the first and second subbands, respectively. The superscript m represents the subbands in the presence of an electric field of 50 kV/cm, and the curves X denote the silicon content in the graded superlattice labeled by the right ordinate.

pure Si region contributes little to the in-plane birefringence because of the same type of chemical bond there. Thus, the in-plane anisotropy may arise only from the optical transitions in the graded region of Si_xGe_{1-x}.

Another decisive factor determining the biaxial response is the difference between the neighboring [110] and [$\bar{1}$10] oriented chemical bonds. In the graded Si_xGe_{1-x} region, along the [001] direction the chemical bonds vary as the x profile varies, which affects the difference between chemical bonds with different orientations in the vicinity of a monolayer. Therefore, in addition to the barrier penetration of the wave functions, the in-plane optical anisotropy will critically depend on the variation rate of profile x in the graded regions.

In the presence of an external electric field, the electron and hole will polarize oppositely. As shown in Fig. 7(b), the envelope functions of the first two conduction subbands shift to the left significantly, while the first two valence subbands moves to the right slightly. The redistribution of the envelope functions changes the electron-hole overlap in the Si_xGe_{1-x} layers, resulting in the variation of the in-plane anisotropy, i.e., quantum confined Pockels effect.

Comparing the envelope functions of the first and second valence/conduction subbands in three types of graded superlattices (Fig. 7), it is obvious that the profile form in the graded layers affects distribution of holes rather small, but influences the electrons significantly. The electron penetration in the parabola (antiparabola) superlattice is stronger (weaker) than that in the sawtooth superlattice. Hence, the overlap integral in the graded layers of the parabola is the largest, and that in the antiparabola is the smallest. On the other hand, the difference of chemical bonds along the [001] direction depend on the derivative of the profile function, which takes its turn from antiparabola, sawtooth, and parabola, with antiparabola as the biggest. Combining these two factors together, it is not surprising that the quantum confined Pockels effect in the sawtooth superlattice is the most prominent.

V. CONCLUSION

In conclusion, taking the accumulated strain effect into account, we have proposed the mended VCA in the empirical

pseudopotential calculation for the energy band as applied to the strained superlattices of the long period. In this way, we confirmed the enhanced quantum confined Pockels effect in the $Si/Si_{0.75}Ge_{0.25}/Si_{0.5}Ge_{0.5}$ trilayer superlattice. The enhanced Pockels effect can be attributed to the type II optical transitions associated with different chemical bonds with [110] and [$\bar{1}$10] orientations adjacent to the $Si_{0.5}Ge_{0.5}$-Si interface, and the different response of electrons and holes to the electrical field. The dependence of the Pockels coefficient on the layer thickness is studied and an optimized structure with a maximum value of Pockels coefficient is reached. Moreover, we propose three types of graded-Si_xGe_{1-x}/Si superlattices grown on the (001) Si substrate, which is expected to exhibit stronger quantum confined Pockels effect. Based on the electronic structure calculation, the enhanced Pockels coefficients are attributed to the type II indirect optical transitions in the graded region of Si_xGe_{1-x}. The dependence of the Pockels coefficient on the profiles of x in three types of graded layers is studied, suggesting an optimized structure with a sawtooth profile, which might be the candidate for application of silicon-based materials in optoelectronics and photonics.

[1] T. P. Pearsall, J. M. Vandenberg, R. Hull, and J. M. Bonar, Phys. Rev. Lett. **63**, 2104 (1989).

[2] M. Gell, Phys. Rev. B **40**, 1966 (1989).

[3] S. Satpathy, R. M. Martin, and C. G. Van de Walle, Phys. Rev. B **38**, 13237 (1988).

[4] C. Tserbak and G. Theodorou, Phys. Rev. B **50**, 18179 (1994).

[5] E. Ghahramani, D. J. Moss, and J. E. Sipe, Phys. Rev. B **41**, 5112 (1990).

[6] R. W. Boyd, *Nonlinear Optics* (Academic, New York, 1992).

[7] S. H. Kwok, H. T. Grahn, K. Ploog, and R. Merlin, Phys. Rev. Lett. **69**, 973 (1992).

[8] B. F. Zhu and Y. C. Chang, Phys. Rev. B **50**, 11932 (1994).

[9] R. Atanasov, F. Bassani, and V. M. Agranovich, Phys. Rev. B **50**, 7809 (1994).

[10] V. Pellegrini, A. Parlangeli, M. Börger, R. D. Atanasov, F. Beltram, L. Vanzetti, and A. Franciosi, Phys. Rev. B **52**, R5527 (1995).

[11] A. Fiore, E. Rosencher, B. Vinter, D. Weill, and V. Berger, Phys. Rev. B **51**, 13192 (1995).

[12] O. Krebs and P. Voisin, Phys. Rev. Lett. **77**, 1829 (1996).

[13] E. L. Ivchenko, A. Yu. Kaminski, and U. Rössler, Phys. Rev. B **54**, 5852 (1996).

[14] O. Krebs, D. Rondi, J. L. Gentner, L. Goldstein, and P. Voisin, Phys. Rev. Lett. **80**, 5770 (1998).

[15] A. V. Platonov, V. P. Kochereshko, E. L. Ivchenko, G. V. Mikhailov, D. R. Yakovlev, M. Keim, W. Ossau, A. Waag, and G. Landwehr, Phys. Rev. Lett. **83**, 3546 (1999).

[16] B. A. Foreman, Phys. Rev. Lett. **84**, 2505 (2000).

[17] A. A. Toropov, E. L. Ivchenko, O. Krebs, S. Cortez, P. Voisin, and J. L. Gentner, Phys. Rev. B **63**, 035302 (2001).

[18] S. Cortez, O. Krebs, and P. Voisin, Eur. Phys. J. B **21**, 241 (2001).

[19] E. L. Ivchenko and M. O. Nestoklon, Phys. Rev. B **70**, 235332 (2004).

[20] U. Schmid, F. Lukes, N. E. Christensen, M. Alouani, M. Cardona, E. Kasper, H. Kibbel, and H. Presting, Phys. Rev. Lett. **65**, 1933 (1990).

[21] U. Schmid, N. E. Christensen, M. Alouani, and M. Cardona, Phys. Rev. B **43**, 14597 (1991).

[22] M. Ikeda, K. Terakura, and T. Oguchi, Phys. Rev. B **45**, 1496 (1992).

[23] M. Ikeda, K. Terakura, and T. Oguchi, Phys. Rev. B **48**, 1571 (1993).

[24] R. Yu, B. F. Zhu, and Q. M. Wang, J. Phys.: Condens. Matter **13**, L559 (2001).

[25] L. C. LewYanVoon and L. R. Ram-Mohan, Phys. Rev. B **47**, 15500 (1993).

[26] M. Graf and P. Vogl, Phys. Rev. B **51**, 4940 (1995).

[27] T. G. Pedersen, K. Pedersen, and T. B. Kriestensen, Phys. Rev. B **63**, 201101(R) (2001).

[28] C. G. Van de Walle, Phys. Rev. B **39**, 1871 (1989).

[29] R. People, Phys. Rev. B **32**, 1405 (1985).

[30] P. Friedel, M. S. Hybertsen, and M. Schluter, Phys. Rev. B **39**, 7974 (1989).

[31] K. B. Wong, M. Jaros, I. Morrison, and J. P. Hagon, Phys. Rev. Lett. **60**, 2221 (1988).

[32] M. A. Gell and A. C. Churchill, Phys. Rev. B **39**, 10449 (1989).

[33] B. M. Adderley, R. J. Turton, and M. Jaros, Phys. Rev. B **49**, 16622 (1994).

[34] Ian Morrison, M. Jaros, and K. B. Wong, Phys. Rev. B **35**, 9693 (1987).

[35] Since the period of the superlattices calculated in this paper is fixed to be 100 monolayers, the primitive reciprocal lattice vector along the z direction is $\hat{\mathbf{g}}_z = 2\pi/(25a)(0,0,1)$. And the smallest reciprocal lattice vector for the bulk Si(Ge). along the z direction is $\hat{\mathbf{G}}_z = 2\pi/a(0,0,2)$. So totally 50 $\mathbf{g}_z$'s ($\hat{\mathbf{G}}_z/\hat{\mathbf{g}}_z = 50$) are needed in this paper.

[36] B. F. Zhu, Phys. Rev. B **38**, 13316 (1988).

[37] P. Harrison, *Quantum Wells, Wires and Dots: Theoretical and Computational Physics* (Wiley, Chichester, 1999), p. 363.

[38] E. Desurvire, *Erbium-doped Fiber Amplifiers: Principles and Applications* (Wiley, New York, 1994).

[39] For the Kramers-Kronig relation, the cutoff frequency of the integration is chosen to be 20 eV, which is far bigger than the direct absorption edge of Si-based superlattices (~3.0 eV).